

# Pathways for entanglement based quantum communication in the face of high noise

Xiao-Min Hu,<sup>1,2</sup> Chao Zhang,<sup>1,2</sup> Yu Guo,<sup>1,2</sup> Fang-Xiang Wang,<sup>1,2</sup> Wen-Bo Xing,<sup>1,2</sup>  
Cen-Xiao Huang,<sup>1,2</sup> Bi-Heng Liu,<sup>1,2,\*</sup> Yun-Feng Huang,<sup>1,2</sup> Chuan-Feng Li,<sup>1,2,†</sup>  
Guang-Can Guo,<sup>1,2</sup> Xiaoqin Gao,<sup>3,4,5,‡</sup> Matej Pivoluska,<sup>6,7,§</sup> and Marcus Huber<sup>3,¶</sup>

<sup>1</sup>*CAS Key Laboratory of Quantum Information, University of Science and Technology of China, Hefei, 230026, People's Republic of China*

<sup>2</sup>*CAS Center For Excellence in Quantum Information and Quantum Physics, University of Science and Technology of China, Hefei, 230026, People's Republic of China*

<sup>3</sup>*Institute for Quantum Optics and Quantum Information (IQOQI), Austrian Academy of Sciences, Boltzmannngasse 3, 1090 Vienna, Austria*

<sup>4</sup>*Vienna Center for Quantum Science and Technology (VCQ), Faculty of Physics, University of Vienna, Boltzmannngasse 5, 1090 Vienna, Austria*

<sup>5</sup>*Department of physics, University of Ottawa, Advanced Research Complex, 25 Templeton Street, K1N 6N5, Ottawa, ON, Canada*

<sup>6</sup>*Institute of Computer Science, Masaryk University, 602 00 Brno, Czech Republic*

<sup>7</sup>*Institute of Physics, Slovak Academy of Sciences, 845 11 Bratislava, Slovakia*

(Dated: May 3, 2022)

Entanglement based quantum communication offers an increased level of security in practical secret shared key distribution. One of the fundamental principles enabling this security – the fact that interfering with one photon will destroy entanglement and thus be detectable – is also the greatest obstacle. Random encounters of traveling photons, losses and technical imperfections make noise an inevitable part of any quantum communication scheme, severely limiting distance, key rate and environmental conditions in which QKD can be employed. Using photons entangled in their spatial degree of freedom, we show that the increased noise resistance of high-dimensional entanglement, can indeed be harnessed for practical key distribution schemes. We perform quantum key distribution in eight entangled paths at various levels of environmental noise and show key rates that, even after error correction and privacy amplification, still exceed 1 bit per photon pair and furthermore certify a secure key at noise levels that would prohibit comparable qubit based schemes from working.

## I. INTRODUCTION

Quantum key distribution (QKD) [1–5] is one of the most prominent and mature applications of quantum information theory. It can be used to establish a shared and private random bit-string among two parties, that can subsequently be used to encrypt information [6]. There are different levels of security of quantum key distribution, depending on the assumptions placed on each of the devices used. The weakest form are the so-called prepare and measure protocols [1, 7, 8], which assume a trusted source of quantum states in possession of one of the parties, as well as perfectly characterised measurement devices for both parties. Although such assumptions about components of QKD implementation are often reasonable, they open up loopholes which the potential adversary can abuse to perform attacks on the implementation of the protocol [9, 10]. The other extreme is given by so-called device independent quantum key distribution [11–15], where no assumptions are placed on any devices,

except for the privacy of locally generated randomness. Such protocols provide a revolutionary paradigm shift in designing secure QKD protocols, but they remain largely impractical, because they require a loophole-free Bell inequality violations, which can be obtained only in strict laboratory conditions [16–18]. In-between these two extremal cases, there are plenty of scenarios with various levels of trust placed on the devices, which leads to very different practically achievable key rates [19–26]. Entanglement based protocols belong to this last group as they typically assume the entanglement source is in the control of the adversary. This makes entanglement protocols secure against many attacks abusing source imperfections (e.g. photon splitting attack [27, 28]), possible against prepare and measure protocols.

The physical principle ensuring security of quantum key distribution protocols can be intuitively understood from two fundamental facts about of quantum physics. First of all, an unknown quantum state cannot be copied (the famous no-cloning theorem [29–31]) and second a state cannot undergo a measurement procedure without being influenced (this is called a projection postulate of quantum mechanics, see e.g. [32]). So when encoding information in individual quantum systems, it is impossible to intercept and learn information from them, without also revealing one's presence. While this principle enables classically unachievable levels of security, it also presents a serious challenge. Any interaction of these

\* bhliu@ustc.edu.cn

† cfi@ustc.edu.cn

‡ xgao5@uottawa.ca

§ pivoluskamatej@gmail.com

¶ marcus.huber@univie.ac.at

individual quantum systems with an environment, any background photons that are accidentally detected and other imperfections in the devices will manifest as noise in the data. Such environmental noise cannot be distinguished from noise that would result from malicious activity. There are two big challenges of contemporary QKD stemming from noise [33]. First, QKD protocols cannot certify any shared key, if the noise level is above certain threshold. Second, environmental noise significantly affects the achievable key rate of many protocols even in relatively low noise regimes. One of the big remaining challenges of QKD is therefore to design protocols, which can tolerate large amounts of environmental noise and produce large amounts of key in moderate noise regimes.

The potential way to solve both of these challenges by employing high-dimensional degrees of freedom of photons (see [34] for review of this topic) has been proposed as early as 20 years ago [35, 36]. The idea of increased key rate is straightforward – one photon carrying information in  $d$  dimensional degree of freedom (called a *qudit*) can produce as much as  $\log_2 d$  bits of randomness. Simultaneously, in theory, increasing the dimension  $d$  of used quantum systems also increases the amount of tolerable noise [37]. Practical demonstrations of high-dimensional QKD (HDQKD) followed much later. Prepare and measure protocols demonstrated that in low noise regimes one can indeed obtain increased key-rates [38–46]. On the other hand entanglement based HDQKD protocols were achieved only by employing additional assumptions about the distributed state [47], thus compromising the source independence of the protocol, or restricted measurements [48]. Additionally, none of the implementations show exceptionally high noise resistance. This is partially caused by the fact that with increasing the dimensions in real experiment, one inevitably also increases the environmental noise (see [49] for detailed treatment of dimension dependent noise). Further, this increased noise takes an extra toll, as error correction requires more communication in higher dimensions.

In this article we present a first experimental demonstration of an entanglement based HDQKD protocol, which does not impose any assumptions about the distributed state. Additionally, our implementation exhibits strong noise resistance against real physical noise. This is possible thanks to several recent breakthroughs. It was recently shown [50] that high-dimensional entanglement, i.e. entanglement in multiple degrees of freedom can exhibit an increased resistance to real physical noise compared to low-dimensional counterparts. This led to the proposal of a QKD protocol, simultaneously coding in multiple subspaces of high-dimensional states [49], theoretically predicting the possibility of establishing a secure key in the presence of unprecedented noise levels. Last recent breakthrough is the development of experimental setups for creation and manipulation of path entanglement [51], which allow implementation of true multi-outcome measurements with high fidelity. Putting these

ideas together, we implement the protocol introduced in [49] using eight-dimensional path entanglement and bilateral eight-outcome measurements. We show that even after post-processing, the key rate exceeds one bit per coincidence, i.e. each detected pair establishes more key than would be possible to encode in even a perfect and noiseless qubit. Furthermore, we prepare an entire family of states by adding artificial noise to the experiment, fully exploring the achievable noise resistance of the protocol. Our implementation exhibits the behaviour predicted in [49] – high-dimensional subspaces are best when the noise is low, because they achieve superior key rates and low-dimensional subspaces of high-dimensional states offer significant increase in noise-resistance. We therefore for the first time experimentally demonstrate that employing high dimensional photonic degrees of freedom in QKD can both significantly increase key rates and achieve high noise resistance.

## II. RESULTS

In our experiment, we generate and distribute single photon pairs, entangled in their path degree of freedom. Using 8 detectors on each side, we record coincidences between all paths and compute both the secure key generated per selected photon pair (i.e. the average key rate per subspace post-selected coincidence  $K_{BPSC}$ ) and the resulting secure key per second ( $K_{BPS} = K_{BPSC} \times TSCS$ , where  $TSCS$  is the total subspace coincidence per second). These results are plotted in figure 1a) and 1b). The key rate is computed from raw data by following the protocol from Ref. [49] (also described in section IV A) for different levels of physical noise, generated by shining light on each of our photon detectors.

We perform six separate experiments, for 8, 4 and 2 local paths (i.e. local dimensions) and subspace measurements in dimensions 2 and 4. The respective measurements are described in appendix B.

We observe that for low noise, we can obtain much higher key rate  $K_{BPSC}$  by setting the subspace dimension  $k$  higher for the same global dimension  $d$ .

However, with the noise increasing, using the subspaces with lower dimensions leads to stronger noise-robustness. From the experimental results, we can see the key rate  $K_{BPSC}$  of  $k = 4$  decreases rather fast compared to the cases with  $k = 2$ .

Similar results are shown in subspaces with different dimensions when  $d = 4$ . Importantly, the robustness of the protocol also increases with the total dimension  $d$ . For example, the key rate  $K_{BPSC}$  of  $k = 4$  decreases more slowly in  $d = 8$  than in  $d = 4$  and similar observation can be made for  $k = 2$ .

One can notice that for all subspace sizes,  $K_{BPS}$  is effectively doubled when one compares  $d = 8$  to  $d = 4$  and  $d = 2$ . This occurs because doubling  $d$  also doubles the number of entangled pairs generated per second, as more beam paths are collected in detectors.  $TSCS$  therefore

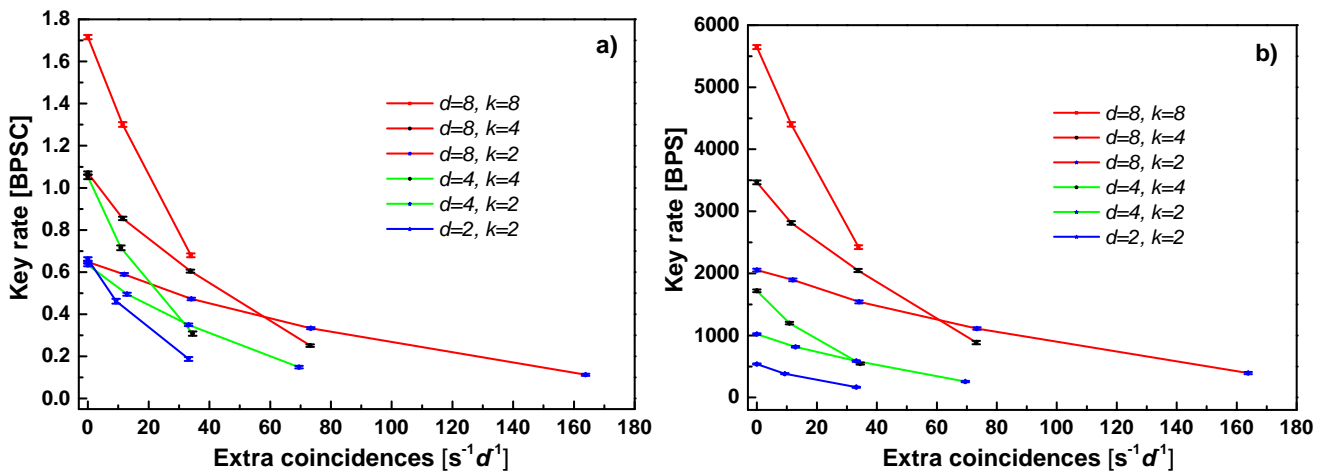


FIG. 1. a) The key rate (bits per subspace post-selected coincidence, BPSC) in the eight/four/two (red/green/blue) -dimensional spaces. Noise is shown as average additional coincidences per second, divided by the local dimension (i.e. 8, 4 and 2 respectively). The points with error bars represent the experimental values obtained by adding different levels of noise. The experimental results show that higher-dimensional subspace coding can increase the key rate  $K_{BPSC}$  significantly at lower noise levels. The optimal noise resistance is always achieved in two-dimensional subspaces for every total dimension  $d$ . Importantly, increasing the number of paths improves key rates for all subspace sizes and noise levels. In particular, qubit encoding has the worst performance in all noisy scenarios b) The key rate (bits per second, BPS) changes with the same tendencies of the key rate  $K_{BPSC}$ . Notably, increasing the dimension allows us to increase the pump strength in this setup (the number of coincidences in 25 seconds is roughly  $d \times 10000$ ), which allows us to increase  $K_{BPSC}$  with the dimension by another physical mechanism. The detailed experimental data are shown in Table VI. of in Appendix D.

increases from  $\approx 800$  pairs per second in case of  $d = 2$  to  $\approx 1600$  pairs per second in case of  $d = 4$  and  $\approx 3200$  pairs per second in case of  $d = 8$  (see Table VI in Appendix D for detailed values of  $TSCS$ ). Note however, that the increase of  $TSCS$  for higher dimensions can be expected also for fundamental reasons. Considering the damage threshold of nonlinear crystals (such as BBO) [52], the permitted maximal pump strength is proportional to the path dimension  $d$  and one can, in principle, create more entangled pairs for higher  $d$ . This is because in path entanglement the crystal is pumped at multiple distinct locations and therefore heated more evenly.

### III. DISCUSSION

The intricate relation between global and subspace dimension shows a clear pathway towards optimal usage of high-dimensional entanglement for quantum communication. While increasing the global dimension improves the achievable key rate and noise resistance simultaneously, it should be noted that it of course comes at the cost of increasing the number of detectors on each side. If we want to increase to even more spatial dimensions, a plausible path towards scaling our scheme would be an introduction of a path-dependent delay for mapping the outcomes from the spatial to the temporal domain (thus eliminating the need for  $d$  detectors, replacing them with one detector and a precise clock). Another interesting factor is the optimal subspace dimension, as it clearly

shows that for low noise levels a high subspace dimension is optimal. On the other hand the noise resistance is achievable with decreasing subspace dimension as a function of noise. In experimental setups with constant signal to noise ratios this implies a single optimal subspace coding. In variable situations, such as complex quantum networks or free space communication it would seem prudent to consider an on-the-fly optimisation of subspace dimension to swiftly adapt to changing conditions. The particular scheme we use for creating spatial entanglement carries another distinct advantage for quantum communication. The fact that we coherently split the beam prior to pumping the crystal means that the pump laser is heating the crystal in a more distributed fashion, allowing for larger crystals and larger pump intensities before a limiting intensity is reached. This increases the potential number of entangled pairs per second and carriers with it the potential to again increase the key rate by another physical mechanism. One should also mention that there are still two very significant pathways to improve the key rate. On the one hand, we use very conservative tests based on the min-entropy for privacy certification that are moreover only based on two mutually unbiased measurements. Extending the methods to von Neumann entropies and implementing more mutually unbiased measurements (see for example [37]) both will increase the certified private bits and noise resistance while using the same experimental parameters.

The last ingredient that allows us to fairly compare the protocols with different total dimension  $d$  in varying

environmental conditions is adding physical noise to the setup in a controlled fashion. This is achieved by putting independent noise sources in front of each optical coupler to introduce white noise, as shown in figure 2 (b) and (c) respectively (see Appendix C for experimental details). These extra sources of noise lead to accidental coincidences in the data, which we use as a measure of physical environmental noise in the setup.

More precisely, we use the number of extra coincidences per second divided by the local dimension as a measure of noise. The reason to use this measure, in favour of a more traditional quantum bit error rate (QBER) (i.e. the fraction of errors in Alice's and Bob's raw key and test strings), is that QBER does not provide a fair comparison of QKD implementations with different total dimension  $d$ . Consider the following example. It can be shown that increasing  $d$  of QKD protocols increases the QBER at which the protocol can still certify a positive key rate [37]. This in theory means that increasing  $d$  should always lead to the increase in noise resistance, which is, however, not observed in practice. The principal reason for this theory/experiment mismatch is that increasing the dimension  $d$  in experiments can in some implementations also significantly increases the QBER, for example due to using extra detectors, which introduce errors via dark counts and inefficiencies (see [49] for more detailed treatment of dimension-dependent noise). Our measure of noise, takes considerations such as these into account, as it is a measure of real physical noise in the experiment – it essentially captures the environmental conditions present in different runs of the protocol. In fact, in Fig. 1, we can observe that our measure captures the physical noise well, as for each tested area of added coincidences per second and local dimension, the physical conditions (the actual light intensity of the noise sources) were the same. Here, one can also see a slight increase of effective noise in higher dimensions, despite equivalent environment conditions. This is because the larger number of detectors also increases the amount of accidental coincidences caused by dark counts.

In conclusion, by implementing the first entanglement based, high-dimensional and multi-outcome QKD experiment, we were able to achieve key rates exceeding 1 bit of perfect key after error correction per photon pair. This significant increase even survived the artificial injection of additional accidentals through ambient light. By increasing the artificial noise, we were also able to demonstrate the superior noise resistance of subspace coding in high-dimensional systems and experimentally explore the intricate relationship between global dimension, subspace dimension, key rate and noise. Our experiment proves the viability of high-dimensional coding for overcoming some of the most significant challenges of quantum communication and identifies novel pathways for noise resistant key distribution.

## IV. MATERIALS AND METHODS

### A. The Protocol

Here we briefly present the high-dimensional entanglement based QKD protocol developed in [49]. The protocol is composed of  $N$  rounds, in which the source distributes a  $d \times d$  entangled state  $\rho_{AB} \in \mathcal{H}_A \otimes \mathcal{H}_B$  to two communicating parties, Alice and Bob. In the ideal case  $\rho_{AB} = |\phi_d^+\rangle\langle\phi_d^+|$ , where  $|\phi_d^+\rangle = \frac{1}{\sqrt{d}} \sum_{i=0}^{d-1} |ii\rangle$  is a maximally entangled state. Postulates of quantum mechanics guarantee that measuring this state by both Alice and Bob in the  $d$  dimensional computational basis (called a *key basis*) leads to two  $\log_2(d)N$ -bit strings  $X$  and  $Y$ . These two strings are uniformly distributed and perfectly correlated and private, thus they constitute a shared secret key. However, any real world implementation is necessarily imperfect and thus the quality of the state  $\rho_{AB}$  needs to be assessed. Particularly, in randomly chosen rounds, Alice and Bob measure the state in a *test basis* which allows them to estimate the amount of key they can distill from their key basis measurement outcomes  $X$  and  $Y$ . This step is then followed by classical post-processing. This is composed of *error correction*, in which differences between  $X$  and  $Y$  are corrected and *privacy amplification*, in which the final key – shorter but uniformly distributed shared string – is obtained. Particular entanglement based QKD protocols differ precisely in how they assess the quality of the key basis measurement data. Here we employ methods developed in [49], where the quality of data obtained in the  $d$ -dimensional key basis is assessed by measurements in a mutually unbiased basis [53]. Formally, for dimension  $d$ , Alice's test measurement is a projective measurement mutually unbiased to the computational measurement.  $\{|m'\rangle\}_{m=0,\dots,d-1}$ , defined as

$$|m'\rangle = \frac{1}{\sqrt{d}} \sum_{j=0}^{d-1} \omega^{mj} |j\rangle, \quad (1)$$

where  $\omega = e^{i2\pi/d}$  and  $\{|j\rangle\}_{j=0,\dots,d-1}$  is the computational basis. Similarly, Bob's test measurement is a projective measurement onto  $\{|m'\rangle^*\}_{m=0,\dots,d-1}$ , where  $*$  denotes complex conjugation. The test rounds of the protocol are then used to assess the following witness:

$$W_d = \sum_{i=0}^{d-1} \Pr(ii|\text{test}), \quad (2)$$

where  $\Pr(ii|\text{test})$  is the probability that both parties simultaneously obtained result  $i$  when measuring in their test basis. This witness can then be turned into a lower bound on the conditional min-entropy, which bounds the information  $E$  the adversary Eve, has about Alice's single measurement outcome in the key basis:

$$H_{\min}(X|E)_{\rho_{AB}} \geq -\log_2 \left( \frac{(\sqrt{W_d} + \sqrt{(d-1)(1-W_d)})^2}{d} \right). \quad (3)$$

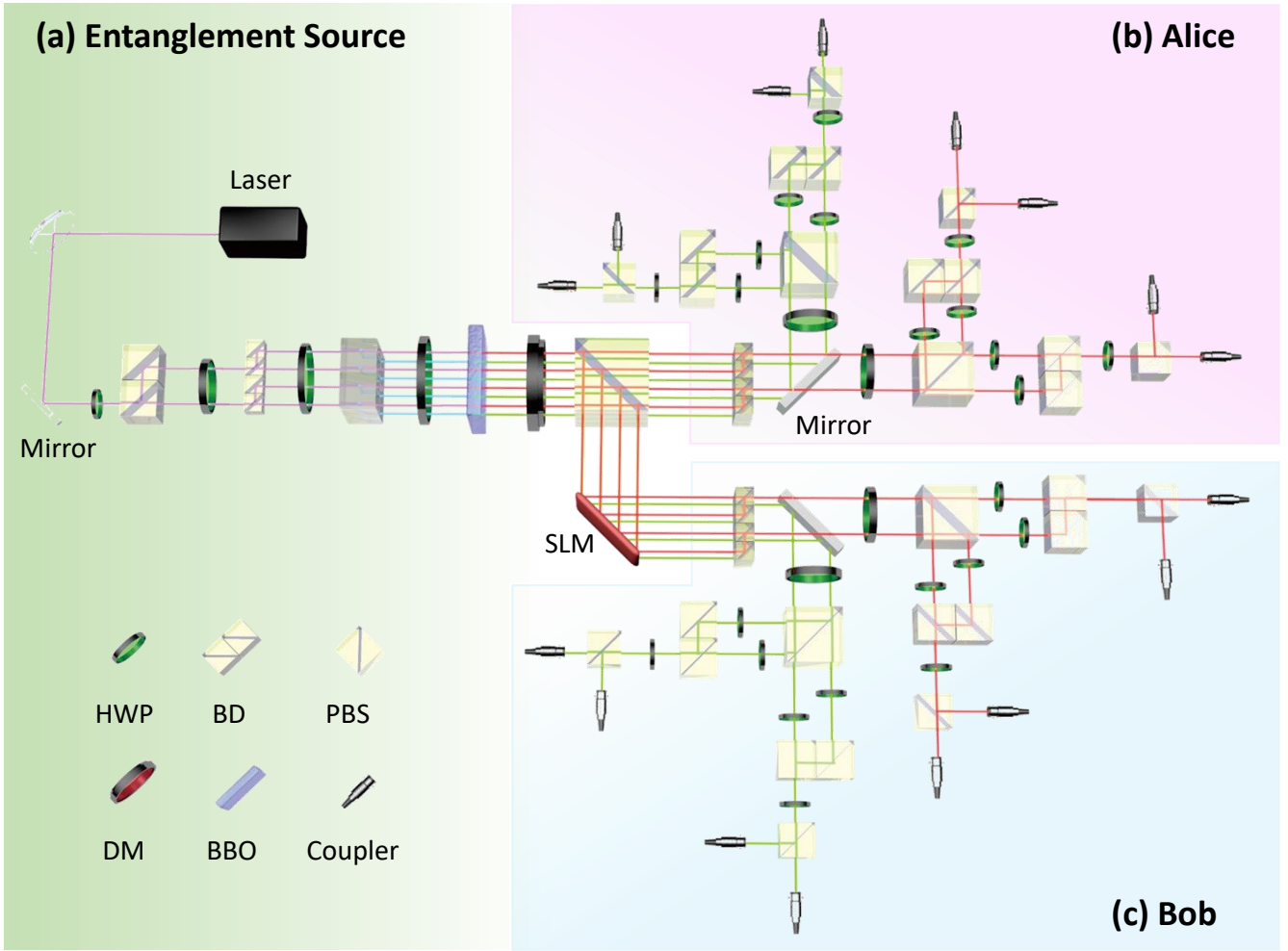


FIG. 2. Experimental setup. (a) Preparation of eight-dimensional entanglement: Eight parallel beams are obtained by eight equal divisions of the pumped continuous-wave light (@ $404\text{ nm}$ , the diameter is  $0.6\text{ mm}$ ), with the help of three half-wave plates (HWPs @ $22.5^\circ$ ) and three beam-displacers (BDs). Eight beams are assigned into two-layer eight paths, the upper layer and the lower layer represented with purple and blue colours respectively, labelled with  $|0\rangle, |1\rangle, \dots, |7\rangle$ . The distance between each path and the neighbouring path is  $2\text{ mm}$ . Another HWP @ $22.5^\circ$  is necessary for all beams to transmit with  $H$  polarization. Finally, an eight-dimensional polarization-based target state  $|\phi_8^+\rangle$  (@ $808\text{ nm}$ ), distributed in red layer and green layer respectively, is prepared by injecting all beams into a BBO crystal ( $|H\rangle_{404\text{nm}} \mapsto |H\rangle_{808\text{nm}} \otimes |V\rangle_{808\text{nm}}$ ) to generate eight pairs of infrared photons via the Type-II spontaneous parametric down-conversion (SPDC). When using only the upper layer, we get a four-dimensional target state  $|\phi_4^+\rangle$ . Similarly working with two paths ( $|0\rangle$  and  $|1\rangle$ ) only we get a two-dimensional target state  $|\phi_2^+\rangle$ . The pump beams are removed by a dichroic mirror (DM) and the two kinds of photons are separated by a polarizing beam splitter (PBS).  $H$  photons are sent to Alice, while  $V$  photons are sent to Bob after using a phase-only spatial light modulator (SLM) to manipulate the phase of incident photons. Parts (b) and (c) of the figure depict multi-outcome measurements for Alice and Bob. The conversion of projective measurements between computational basis (key round of the protocol) and subspace Fourier-transform basis (test round of the protocol) can be realized by changing the angles of HWPs, for details see Appendix B. White noise is introduced by putting independent noise sources before each optical coupler. As an example shown in this experiment with  $d = 8$ , using two mirrors we split the space into two subspaces,  $\{|0\rangle, |1\rangle, |2\rangle, |3\rangle\}$  (red beams in the picture) and  $\{|4\rangle, |5\rangle, |6\rangle, |7\rangle\}$  (green beams in the picture), each subspace has four dimensions.

In turn, min-entropy lower bounds the von Neumann entropy  $H(X|E)_{\rho_{AB}}$ , which together with another experimentally accessible quantity – the conditional Shannon entropy  $H(X|Y)$  between Alice’s and Bob’s key measurement outcomes lower bounds the key rate per coincidence

(in the limit of infinite rounds) as [54, 55]:

$$K \geq H(X|E)_{\rho_{AB}} - H(X|Y) \geq H_{\min}(X|E)_{\rho_{AB}} - H(X|Y). \quad (4)$$

Another key technique that allows QKD in high-noise scenarios was developed in [49]. Whole  $d$  dimensional Hilbert space is divided into  $d/k$  mutually exclusive sub-

spaces of size  $k$ , labelled  $S_1, \dots, S_{d/k}$  and additional round of post-selection is added – Alice and Bob keep the measurement outcomes if and only if, they obtained results in the same subspace. Then the key rate  $K_i$  is obtained separately in each subspace  $S_i$  and the final key rate is obtained as an average of  $d/k$  observed key rates. A  $k$  dimensional protocol is thus in effect run in parallel for  $d/k$  subspaces. In order to run this modified protocol we need to redefine the test measurement basis, such that we are projecting onto mutually unbiased basis in each subspace. For each subspace  $S_i$  spanned by computational basis vectors  $|i_0\rangle, \dots, |i_{k-1}\rangle$  and  $m \in \{0, \dots, k-1\}$  we define a set of mutually unbiased vectors  $|m_i\rangle = \frac{1}{\sqrt{k}} \sum_{j=0}^{k-1} \omega_k^{mj} |i_j\rangle$ , where  $\omega_k = e^{i2\pi/k}$ . Collection of  $d$  vectors  $\{|m_i\rangle | m \in \{0, \dots, k-1\}, i \in \{1, \dots, d/k\}\}$  constitutes a basis of the whole  $d$  dimensional Hilbert space and thus defines a projective measurement. In the subspace protocol Alice uses this measurement as her test measurement and Bob uses  $\{|m_i\rangle^* | m \in \{0, \dots, k-1\}, i \in \{1, \dots, d/k\}\}$ , where  $*$  denotes complex conjugation. A measurement result  $|m_i\rangle$  is then interpreted as outcome  $m$  in subspace  $S_i$ .

## B. Preparation of high-dimensional entangled state and multi-outcome complete measurement

In our experiment, we aim at creating a maximally entangled state in  $d$ -dimensions using path entanglement. To fully explore the high noise regime in a controlled manner, we shine ambient light on each detector, leading to accidental coincidences that we count per detector for a fair bookkeeping.

To explore the interplay of global and subspace dimensions, we study three cases of global dimension  $d = 8$ ,  $d = 4$  and  $d = 2$ , with subspace dimensions  $k = 2, 4$  and  $8$ . For preparing the eight-dimensional target state  $|\phi_8^+\rangle$ , encoded in the path degree of freedom, we use three half-wave plates (HWPs) @22.5° together with three beam-displacers (BDs). Eight parallel beams are distributed to eight paths with the same energy by dividing the pumped light equally. Pumped light is produced by a continuous-

wave diode laser @404 nm, as shown in figure 2 (a). Let us label eight paths as  $|0\rangle, |1\rangle, \dots, |7\rangle$  distributed in two layers. In figure 2 they are marked with purple and blue colours respectively. An additional HWP @22.5° is used to rotate the polarization to be horizontal, allowing them to pump a collinear degenerate SPDC in a Type-II BBO crystal ( $|H\rangle_{404nm} \mapsto |H\rangle_{808nm} \otimes |V\rangle_{808nm}$ ) to generate eight polarization-based photon pairs @808 nm located in two layers distinguished by red and green colours respectively. Remarkably, it is easy to prepare the four-dimensional target state  $|\phi_4^+\rangle$  if we only consider the upper layer (marked red in figure 2). Afterwards, a dichroic mirror (DM) is used to filter out the pump beams and a polarizing beam splitter (PBS) is applied to send horizontally polarized photons to Alice and vertically polarized photons to Bob respectively. To compensate for the phase between Alice and Bob, a spatial light modulator (SLM) is added to implement an arbitrary phase on the vertically polarised light [51].

In our setup we use polarization to control the path degree of freedom in order to implement 8-outcome measurements required for the protocol. Note, however, that in principle, our multi-outcome measurement technique can be generalized to higher dimensions effectively [51]. By changing the angles of HWPs placed in parts (b) and (c) of figure 2, Alice and Bob can switch between the projective measurements used in the protocol (see Appendix B for details). Due to current limitations on the parallelism of beams in the BD, the mutually unbiased basis in dimension 8 would not reach the desired fidelity, a fact that will in the future be mitigated by improvements in BD manufacturing. Nonetheless, we managed to generalise the protocol to work with mutually unbiased subspace measurements with overlapping subspaces to certify security in 8 dimensions, even without fully mutually unbiased measurements as described in the original protocol (see Appendix A for details).

## V. REFERENCES

- 
- [1] C. H. Bennett and G. Brassard, *Theoretical Computer Science* **560**, 7 (2014), theoretical Aspects of Quantum Cryptography – celebrating 30 years of BB84.
  - [2] A. K. Ekert, *Phys. Rev. Lett.* **67**, 661 (1991).
  - [3] V. Scarani, H. Bechmann-Pasquinucci, N. J. Cerf, M. Dušek, N. Lütkenhaus, and M. Peev, *Rev. Mod. Phys.* **81**, 1301 (2009).
  - [4] H.-K. Lo, M. Curty, and K. Tamaki, *Nature Photonics* **8**, 595 (2014).
  - [5] S. Pirandola, U. L. Andersen, L. Banchi, M. Berta, D. Bunandar, R. Colbeck, D. Englund, T. Gehring, C. Lupo, C. Ottaviani, J. Pereira, M. Razavi, J. S. Shaari, M. Tomamichel, V. C. Usenko, G. Vallone, P. Villoresi, and P. Wallden, arXiv e-prints, arXiv:1906.01645 (2019), arXiv:1906.01645 [quant-ph].
  - [6] H. Delfs and H. Knebl, “Symmetric-key cryptography,” in *Introduction to Cryptography: Principles and Applications* (Springer Berlin Heidelberg, Berlin, Heidelberg, 2015) pp. 11–48.
  - [7] D. Bruß, *Phys. Rev. Lett.* **81**, 3018 (1998).
  - [8] C. H. Bennett, *Phys. Rev. Lett.* **68**, 3121 (1992).
  - [9] L. Lydersen, C. Wiechers, C. Wittmann, D. Elser, J. Skaar, and V. Makarov, *Nature photonics* **4**, 686 (2010).
  - [10] Y.-J. Qian, D.-Y. He, S. Wang, W. Chen, Z.-Q. Yin, G.-C. Guo, and Z.-F. Han, *Physical Review Applied* **10**,

- 064062 (2018).
- [11] S. Pironio, A. Acín, N. Brunner, N. Gisin, S. Massar, and V. Scarani, *New Journal of Physics* **11**, 045021 (2009).
- [12] U. Vazirani and T. Vidick, *Phys. Rev. Lett.* **113**, 140501 (2014).
- [13] C. A. Miller and Y. Shi, *J. ACM* **63** (2016), 10.1145/2885493.
- [14] R. Arnon-Friedman, R. Renner, and T. Vidick, *SIAM Journal on Computing* **48**, 181 (2019).
- [15] G. Murta, S. B. van Dam, J. Ribeiro, R. Hanson, and S. Wehner, *Quantum Science and Technology* **4**, 035011 (2019).
- [16] B. Hensen, H. Bernien, A. E. Dréau, A. Reiserer, N. Kalb, M. S. Blok, J. Ruitenbergh, R. F. Vermeulen, R. N. Schouten, C. Abellán, *et al.*, *Nature* **526**, 682 (2015).
- [17] L. K. Shalm, E. Meyer-Scott, B. G. Christensen, P. Bierhorst, M. A. Wayne, M. J. Stevens, T. Gerrits, S. Glancy, D. R. Hamel, M. S. Allman, *et al.*, *Physical review letters* **115**, 250402 (2015).
- [18] M. Giustina, M. A. Versteegh, S. Wengerowsky, J. Handsteiner, A. Hochrainer, K. Phelan, F. Steinlechner, J. Kofler, J.-Å. Larsson, C. Abellán, *et al.*, *Physical review letters* **115**, 250401 (2015).
- [19] H.-K. Lo, M. Curty, and B. Qi, *Phys. Rev. Lett.* **108**, 130503 (2012).
- [20] M. Pawłowski and N. Brunner, *Phys. Rev. A* **84**, 010302 (2011).
- [21] C. Branciard, E. G. Cavalcanti, S. P. Walborn, V. Scarani, and H. M. Wiseman, *Phys. Rev. A* **85**, 010301 (2012).
- [22] X. Ma and M. Razavi, *Phys. Rev. A* **86**, 062319 (2012).
- [23] Y. Liu, T.-Y. Chen, L.-J. Wang, H. Liang, G.-L. Shentu, J. Wang, K. Cui, H.-L. Yin, N.-L. Liu, L. Li, X. Ma, J. S. Pelc, M. M. Fejer, C.-Z. Peng, Q. Zhang, and J.-W. Pan, *Phys. Rev. Lett.* **111**, 130502 (2013).
- [24] H.-L. Yin, T.-Y. Chen, Z.-W. Yu, H. Liu, L.-X. You, Y.-H. Zhou, S.-J. Chen, Y. Mao, M.-Q. Huang, W.-J. Zhang, H. Chen, M. J. Li, D. Nolan, F. Zhou, X. Jiang, Z. Wang, Q. Zhang, X.-B. Wang, and J.-W. Pan, *Phys. Rev. Lett.* **117**, 190501 (2016).
- [25] M. Curty, F. Xu, W. Cui, C. C. W. Lim, K. Tamaki, and H.-K. Lo, *Nature communications* **5**, 1 (2014).
- [26] S. Pirandola, C. Ottaviani, G. Spedalieri, C. Weedbrook, S. L. Braunstein, S. Lloyd, T. Gehring, C. S. Jacobsen, and U. L. Andersen, *Nature Photonics* **9**, 397 (2015).
- [27] G. Brassard, N. Lütkenhaus, T. Mor, and B. C. Sanders, *Physical Review Letters* **85**, 1330 (2000).
- [28] N. Lütkenhaus and M. Jahma, *New Journal of Physics* **4**, 44 (2002).
- [29] J. L. Park, *Foundations of Physics* **1**, 23 (1970).
- [30] W. K. Wootters and W. H. Zurek, *Nature* **299**, 802 (1982).
- [31] D. Dieks, *Physics Letters A* **92**, 271 (1982).
- [32] M. A. Nielsen and I. L. Chuang, *Quantum Computation and Quantum Information: 10th Anniversary Edition*, 10th ed. (Cambridge University Press, USA, 2011).
- [33] E. Diamanti, H.-K. Lo, B. Qi, and Z. Yuan, *npj Quantum Information* **2**, 16025 (2016).
- [34] D. Cozzolino, B. Da Lio, D. Bacco, and L. K. Oxenløwe, *Advanced Quantum Technologies* **2**, 1900038 (2019).
- [35] H. Bechmann-Pasquinucci and W. Tittel, *Phys. Rev. A* **61**, 062308 (2000).
- [36] N. J. Cerf, M. Bourennane, A. Karlsson, and N. Gisin, *Phys. Rev. Lett.* **88**, 127902 (2002).
- [37] L. Sheridan and V. Scarani, *Phys. Rev. A* **82**, 030301 (2010).
- [38] S. Etcheverry, G. Cañas, E. S. Gómez, W. A. T. Nogueira, C. Saavedra, G. B. Xavier, and G. Lima, *Scientific Reports* **3**, 2316 (2013).
- [39] M. Mirhosseini, O. S. Magaña-Loaiza, M. N. O’Sullivan, B. Rodenburg, M. Malik, M. P. J. Lavery, M. J. Padgett, D. J. Gauthier, and R. W. Boyd, *New Journal of Physics* **17**, 033033 (2015).
- [40] G. Cañas, N. Vera, J. Cariñe, P. González, J. Cardenas, P. W. R. Connolly, A. Przysieszna, E. S. Gómez, M. Figueroa, G. Vallone, P. Villorosi, T. F. da Silva, G. B. Xavier, and G. Lima, *Phys. Rev. A* **96**, 022317 (2017).
- [41] N. T. Islam, C. C. W. Lim, C. Cahall, J. Kim, and D. J. Gauthier, *Science advances* **3**, e1701491 (2017).
- [42] A. Sit, F. Bouchard, R. Fickler, J. Gagnon-Bischoff, H. Larocque, K. Heshami, D. Elser, C. Peuntinger, K. Günthner, B. Heim, C. Marquardt, G. Leuchs, R. W. Boyd, and E. Karimi, *Optica* **4**, 1006 (2017).
- [43] Y. Ding, D. Bacco, K. Dalgaard, X. Cai, X. Zhou, K. Rottwitt, and L. K. Oxenløwe, *npj Quantum Information* **3**, 25 (2017).
- [44] D. Cozzolino, D. Bacco, B. Da Lio, K. Ingerslev, Y. Ding, K. Dalgaard, P. Kristensen, M. Galili, K. Rottwitt, S. Ramachandran, and L. K. Oxenløwe, *Phys. Rev. Applied* **11**, 064058 (2019).
- [45] N. T. Islam, C. C. W. Lim, C. Cahall, B. Qi, J. Kim, and D. J. Gauthier, *Quantum Science and Technology* **4**, 035008 (2019).
- [46] I. Vagniluca, B. Da Lio, D. Rusca, D. Cozzolino, Y. Ding, H. Zbinden, A. Zavatta, L. K. Oxenløwe, and D. Bacco, *Phys. Rev. Applied* **14**, 014051 (2020).
- [47] T. Zhong, H. Zhou, R. D. Horansky, C. Lee, V. B. Verma, A. E. Lita, A. Restelli, J. C. Bienfang, R. P. Mirin, T. Gerrits, S. W. Nam, F. Marsili, M. D. Shaw, Z. Zhang, L. Wang, D. Englund, G. W. Wornell, J. H. Shapiro, and F. N. C. Wong, *New Journal of Physics* **17**, 022002 (2015).
- [48] S. Gröblacher, T. Jennewein, A. Vaziri, G. Weihs, and A. Zeilinger, *New Journal of Physics* **8**, 75 (2006).
- [49] M. Doda, M. Huber, G. Murta, M. Pivoluska, M. Plesch, and C. Vlachou, “Quantum key distribution overcoming extreme noise: simultaneous subspace coding using high-dimensional entanglement,” (2020), [arXiv:2004.12824](https://arxiv.org/abs/2004.12824) [quant-ph].
- [50] S. Ecker, F. Bouchard, L. Bulla, F. Brandt, O. Kohout, F. Steinlechner, R. Fickler, M. Malik, Y. Guryanova, R. Ursin, and M. Huber, *Phys. Rev. X* **9**, 041042 (2019).
- [51] X.-M. Hu, W.-B. Xing, B.-H. Liu, Y.-F. Huang, C.-F. Li, G.-C. Guo, P. Erker, and M. Huber, *Phys. Rev. Lett.* **125**, 090503 (2020).
- [52] Y.-F. Huang, B.-H. Liu, L. Peng, Y.-H. Li, L. Li, C.-F. Li, and G.-C. Guo, *Nature Communications* **2**, 546 (2011).
- [53] I. Bengtsson, G. Adenier, C. A. Fuchs, and A. Y. Khrennikov, *AIP Conference Proceedings* **889**, 40 (2007), <https://aip.scitation.org/doi/pdf/10.1063/1.2713445>.
- [54] I. Devetak and A. Winter, *Proceedings of the Royal Society of London Series A* **461**, 207 (2005), [arXiv:quant-ph/0306078](https://arxiv.org/abs/quant-ph/0306078) [quant-ph].
- [55] R. Renner, *Security of quantum key distribution* (Diss., Naturwissenschaften, ETH Zürich, Nr. 16242, 2006, 2005).

## VI. ACKNOWLEDGEMENTS

This work was supported by the National Key Research and Development Program of China (No. 2017YFA0304100, No. 2016YFA0301300 and No. 2016YFA0301700), National Natural Science Foundation of China (Nos. 11774335, 11734015, 11874345, 11821404, 11904357), the Key Research Program of Frontier Sciences, CAS (No. QYZDY-SSW-SLH003), Science Foundation of the CAS (ZDRW-XH-2019-1), the Fundamental Research Funds for the Central Universities, Science and Technological Fund of Anhui Province for Outstanding Youth (2008085J02), Anhui Initiative in Quantum Information Technologies (Nos. AHY020100, AHY060300). X.G. acknowledges the support of Austrian Academy of Sciences (ÖAW) and Joint Centre for Extreme Photonics (JCEP). M.H. acknowledges funding from the Austrian Science Fund (FWF) through the STARTproject Y879-N27. M.P. acknowledges the support of VEGA project 2/0136/19 and GAMU project MUNI/G/1596/2019.



### Appendix A: Calculating key rate in $d = 8, k = 8$

While for  $d = 8$ , direct implementation of the Fourier basis with  $k = 8$  was too noisy in our implementation, we developed another method for certifying security with 8-outcome measurements. By measuring projections onto different global bases  $(|a\rangle \pm |b\rangle) \otimes (|a\rangle \pm |b\rangle)$  and  $(|a\rangle \pm i|b\rangle) \otimes (|a\rangle \pm i|b\rangle)$  for each pair of modes  $a < b$  (i.e. 56 different measurement settings), we are able to directly lower bound the fidelity  $F_+$  of the experimental state  $\rho$  to the maximally entangled state  $|\phi^+\rangle$ . This method was developed in [51]. Recall that in order to estimate the information of the adversary about Alice's measurement results in the computational basis, we need to lower bound the witness

$$W_8 = \sum_{i=0}^7 \langle \tilde{i}i^* | \rho | \tilde{i}i^* \rangle, \quad (\text{A1})$$

where  $|\tilde{i}\rangle$  is a basis mutually unbiased to the computational basis in  $d = 8$  case. Here we utilize the fact that  $\rho$  can be decomposed as  $\rho = F_+ (|\phi^+\rangle\langle\phi^+|) + (1 - F_+) \rho^\perp$ , therefore

$$\begin{aligned} W_8 &= \sum_{i=0}^7 \langle \tilde{i}i^* | \rho | \tilde{i}i^* \rangle \\ &= \sum_{i=0}^7 F_+ \langle \tilde{i}i^* | \phi^+ \rangle \langle \phi^+ | \tilde{i}i^* \rangle + (1 - F_+) \langle \tilde{i}i^* | \rho^\perp | \tilde{i}i^* \rangle \\ &= F_+ + (1 - F_+) \langle \tilde{i}i^* | \rho^\perp | \tilde{i}i^* \rangle \\ &\geq F_+, \end{aligned}$$

where the last inequality holds because  $(1 - F_+) \langle \tilde{i}i^* | \rho^\perp | \tilde{i}i^* \rangle$  is a positive number. This bound can directly be used to estimate  $H_{\min}(X|E)_{\rho_{AB}}$  as

$$H_{\min}(X|E)_{\rho_{AB}} \geq -\log_2 \left( \frac{(\sqrt{W_8} + \sqrt{7(1-W_8)})^2}{8} \right). \quad (\text{A2})$$

In order to obtain the key rate we also need to calculate the amount of information Alice needs to share in order to perform the error correction  $H(A|B)$ . This is accessible directly through the measurement outcomes in the computational basis in the  $d = 8$  case.

### Appendix B: Multi-outcome measurement

Path entanglement has shown its advantages, such as it is possible to implement non-trivial  $d$ -outcome measurements. Here we introduce how to construct a four-outcome and eight-outcome measurement in our experiment. We construct the computational basis  $(\{|0\rangle, |1\rangle, |2\rangle, |3\rangle\})$  and Fourier basis  $(|m_i\rangle = \frac{1}{\sqrt{4}} \sum_{j=0}^3 \omega_k^{mj} |i_j\rangle)$ , where  $\omega_k = e^{i2\pi/k}$ .) for the four-dimensional MUB, as shown in figure 3(a). We use a polarizer to control the path degree of freedom, a HWP1 is used to control the polarizations of paths  $|0\rangle, |1\rangle, |2\rangle$  and  $|3\rangle$ , which encode polarizations of  $V, H, V$  and  $H$  respectively. Via BD1, paths  $|0\rangle, |1\rangle$  and  $|2\rangle, |3\rangle$  are distributed into two polarization-based subspaces respectively. Then HWP1 and PBS1 are used to complete the MUB measurement for two polarization-based two-dimensional subspaces. The results are used to measure the MUB of each two-dimensional subspace by the sets of  $\{\text{BD2, HWP2, PBS2}\}$  and  $\{\text{BD3, HWP3, PBS3}\}$  respectively. The four-dimensional MUB measurement can be completed after two levels of two-dimensional subspace coherent measurements. Importantly, through the measurement of cascaded two-dimensional subspace, of any  $2^n$ -dimensional MUB measurement can be completed. For  $d=2$  MUB measurement, we only use  $|0\rangle$  and  $|1\rangle$  path state, therefore we only need two detectors D1 and D3. The angles of the HWPs are set in table I. For implementing the projective measurements of the QKD protocol presented in figure 3 in main text, the angles of HWPs are set in tables I, II, III, IV and V.

Due to the current limitations on the parallelism of beams in BD, the MUB in eight or higher dimensions can not reach the desired fidelity, it can be improved by enhancing the BD technology in future. Therefore, in our experiment, we only complete  $k = 2$  and 4-dimensional subspace outcome measurements in the global space  $d = 8$ . Instead of measuring the eight-dimensional MUB, we do many measurements in its two-dimensional subspace. For the case  $d = 8, k = 4$ , we use a mirror to separate the global space into two four-dimensional subspaces distributed into upper and lower layers. Then the 4-dimensional subspace MUB is obtained. Notably, the coincidence efficiency of entangled states is roughly 15% without noise. With loading noise, the coincidence efficiency will decrease rapidly.

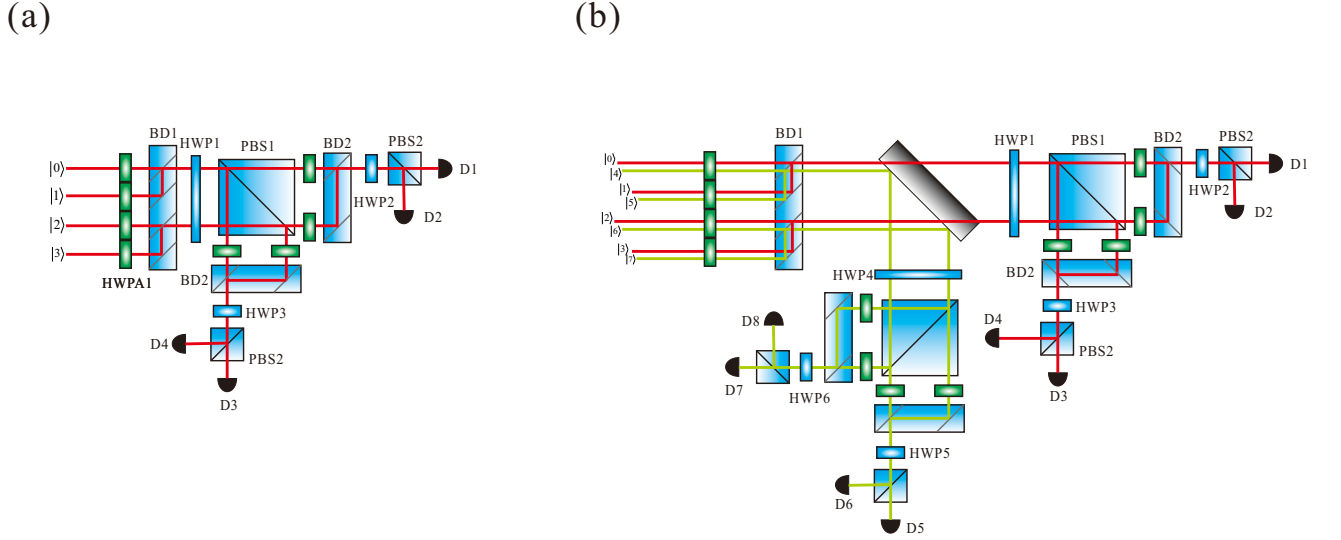


FIG. 3. Four and eight-outcome measurement setups. (a) Four-outcome measurement setup. With adjusting the angles of HWPs (1-3), the computational basis and Fourier-transform basis of  $k = 2, 4$  subspace can be realized. For details, see Tables II and III. (b) Eight-outcome measurement setup. Via adjusting the angles of HWPs (1-6), the computational basis and Fourier-transform basis of  $k = 2, 4$  subspace can be realized. Eight beams distribute in upper and lower layers marked with red and green colors respectively. Only the upper layer is used for the four-outcome measurement setup. For details, see Tables IV and V.

### Appendix C: Loading noise

In our experiment, in order to simulate the noise in the environment, we put sixteen light sources before 16 couplers independently to load a certain amount of noise on each detector. Assuming the single-channel count of each detector is  $S$ , the coincidence count ( $C$ ) for any two detectors between Alice and Bob is obtained, as follows:

$$C = 2 \times S \times S \times \tau \quad (\text{C1})$$

where  $\tau$  is the coincidence window. In our experiment,  $\tau = 5 \times 10^{-9} s$  and we can add any proportion of white noise.

Notably, in the interpretation of results, we calculate the added coincidences from the experimental data – each 25 s run of the protocol is performed at a certain noise level. We subtract the total number of coincidences in the noiseless run from each noisy run to obtain extra coincidences. Then the additional coincidences per second are divided by the local dimension  $d$ , which result in the added coincidence counts plotted in figures.

TABLE I. Measurement for  $d = 2, k = 2$

<i>Computational basis</i>		
HWP1 45°	HWP2 45°	HWP3 45°
D1 $ 0\rangle$		D3 $ 2\rangle$
<i>Fourier-transform basis</i>		
HWP1 22.5°	HWP2 45°	HWP3 45°
D1 $\frac{1}{\sqrt{2}}( 0\rangle +  1\rangle)$		D3 $\frac{1}{\sqrt{2}}( 0\rangle -  1\rangle)$

TABLE II. Measurement for  $d = 4, k = 4$ 

<i>Computational basis</i>			
HWP1 45°	HWP2 45°	HWP3 0°	
D1  0⟩	D2  2⟩	D3  1⟩	D4  3⟩
<i>Fourier-transform basis</i>			
HWP1 22.5°	HWP2 22.5°	HWP3 22.5°	
D1 $\frac{1}{2}( 0\rangle +  1\rangle +  2\rangle +  3\rangle)$	D2 $\frac{1}{2}( 0\rangle +  1\rangle -  2\rangle -  3\rangle)$	D3 $\frac{1}{2}( 0\rangle -  1\rangle +  2\rangle -  3\rangle)$	D4 $\frac{1}{2}( 0\rangle -  1\rangle -  2\rangle +  3\rangle)$

TABLE III. Measurement for  $d = 4, k = 2$ 

<i>Computational basis</i>			
HWP1 45°	HWP2 45°	HWP3 45°	
D1  0⟩	D2  2⟩	D3  1⟩	D4  3⟩
<i>Fourier-transform basis</i>			
HWP1 22.5°	HWP2 45°	HWP3 45°	
D1 $\frac{1}{\sqrt{2}}( 0\rangle +  1\rangle)$	D2 $\frac{1}{\sqrt{2}}( 2\rangle +  3\rangle)$	D3 $\frac{1}{\sqrt{2}}( 0\rangle -  1\rangle)$	D4 $\frac{1}{\sqrt{2}}( 2\rangle -  3\rangle)$

TABLE IV. Measurement for  $d = 8, k = 4$ 

<i>Computational basis</i>							
HWP1 45°	HWP2 45°	HWP3 45°	HWP4 45°	HWP5 45°	HWP6 45°		
D1  0⟩	D2  2⟩	D3  1⟩	D4  3⟩	D5  4⟩	D6  6⟩	D7  5⟩	D8  7⟩
<i>Fourier-transform basis</i>							
HWP1 22.5°	HWP2 22.5°	HWP3 22.5°	HWP4 22.5°	HWP5 22.5°	HWP6 22.5°		
D1 $\frac{1}{2}( 0\rangle +  1\rangle +  2\rangle +  3\rangle)$	D2 $\frac{1}{2}( 0\rangle +  1\rangle -  2\rangle -  3\rangle)$	D3 $\frac{1}{2}( 0\rangle -  1\rangle +  2\rangle -  3\rangle)$	D4 $\frac{1}{2}( 0\rangle -  1\rangle -  2\rangle +  3\rangle)$		D5 $\frac{1}{2}( 4\rangle +  5\rangle +  6\rangle +  7\rangle)$		
D6 $\frac{1}{2}( 4\rangle +  5\rangle -  6\rangle -  7\rangle)$		D7 $\frac{1}{2}( 4\rangle -  5\rangle +  6\rangle -  7\rangle)$		D8 $\frac{1}{2}( 4\rangle -  5\rangle -  6\rangle +  7\rangle)$			

TABLE V. Measurement for  $d = 8, k = 2$ 

<i>Computational basis</i>							
HWP1 45°	HWP2 45°	HWP3 45°	HWP4 45°	HWP5 45°	HWP6 45°		
D1  0⟩	D2  2⟩	D3  1⟩	D4  3⟩	D5  4⟩	D6  6⟩	D7  5⟩	D8  7⟩
<i>Fourier-transform basis</i>							
HWP1 22.5°	HWP2 45°	HWP3 45°	HWP4 22.5°	HWP5 45°	HWP6 45°		
D1 $\frac{1}{\sqrt{2}}( 0\rangle +  1\rangle)$	D2 $\frac{1}{\sqrt{2}}( 2\rangle +  3\rangle)$		D3 $\frac{1}{\sqrt{2}}( 0\rangle -  1\rangle)$		D4 $\frac{1}{\sqrt{2}}( 2\rangle -  3\rangle)$		
D5 $\frac{1}{\sqrt{2}}( 4\rangle +  5\rangle)$		D6 $\frac{1}{\sqrt{2}}( 6\rangle +  7\rangle)$		D7 $\frac{1}{\sqrt{2}}( 4\rangle -  5\rangle)$		D8 $\frac{1}{\sqrt{2}}( 6\rangle -  7\rangle)$	

### Appendix D: Experimental results

Table VI contains detailed data represented in figures in the main text. NOISE means the average noise coincidences per second divided by the local dimension  $d$ , thus representing extra coincidences one can assign to each of Alice's detectors. BPSC denotes key rate in bits per subspace coincidence, TSCS denotes total number of subspace coincidences per second and BPS denotes key rate in bits per second.

TABLE VI. Key rate for different subspace coding

<b><math>d = 8, k = 8</math></b>					
NOISE	0	11.44	33.915	74.755	164.23
BPSC	$1.716 \pm 0.010$	$1.301 \pm 0.011$	$0.680 \pm 0.009$	0	0
TSCS	3291.88	3383.4	3563.2	3889.92	4605.72
BPS	$5648 \pm 33$	$4402 \pm 37$	$2423 \pm 32$	0	0
<b><math>d = 8, k = 4</math></b>					
NOISE	0	11.45	33.735	73.1575	164.735
BPSC	$1.070 \pm 0.008$	$0.855 \pm 0.008$	$0.605 \pm 0.007$	$0.252 \pm 0.006$	0
TSCS	3240.08	3290.12	3380.52	3520.92	3896
BPS	$3468 \pm 30$	$2813 \pm 29$	$2046 \pm 26$	$886 \pm 26$	0
<b><math>d = 8, k = 2</math></b>					
NOISE	0	11.995	34.065	73.3725	163.845
BPSC	$0.648 \pm 0.007$	$0.590 \pm 0.006$	$0.473 \pm 0.006$	$0.334 \pm 0.005$	$0.113 \pm 0.005$
TSCS	3169.48	3215.8	3260.48	3329.8	3486.2
BPS	$2054 \pm 23$	$1897 \pm 22$	$1541 \pm 22$	$1112 \pm 20$	$393 \pm 19$
<b><math>d = 4, k = 4</math></b>					
NOISE	0	10.825	34.47	73.615	
BPSC	$1.053 \pm 0.011$	$0.715 \pm 0.011$	$0.309 \pm 0.010$	0	
TSCS	1633.4	1675.36	1770.68	1925.56	
BPS	$1720 \pm 21$	$1199 \pm 19$	$546 \pm 17$	0	
<b><math>d = 4, k = 2</math></b>					
NOISE	0	12.855	33.16	69.485	
BPSC	$0.635 \pm 0.007$	$0.495 \pm 0.007$	$0.350 \pm 0.006$	$0.149 \pm 0.006$	
TSCS	1610.56	1647.64	1677.68	1736.48	
BPS	$1022 \pm 13$	$816 \pm 13$	$587 \pm 12$	$258 \pm 11$	
<b><math>d = 2, k = 2</math></b>					
NOISE	0	9.26	33.17	65.57	164.53
BPSC	$0.661 \pm 0.010$	$0.462 \pm 0.011$	$0.188 \pm 0.009$	0	0
TSCS	816.44	832.4	882.52	935.6	1141.12
BPS	$540 \pm 8$	$385 \pm 9$	$166 \pm 9$	0	0